THE THERMAL PROPERTIES OF WATER-BASED HYBRID NANOFLUID ($Cu-Al_2O_3$) BEYOND AN INCLINED PLANE

by

Nadia Diana MOHD RUSDI [a], ***Siti Suzilliana Putri Mohamed ISA*** [a,b*], ***Norihan Md. ARIFIN*** [a,c], **and** ***Norfifah BACHOK*** [a,c]

[a] Institute for Mathematical Research (INSPEM), Universiti Putra Malaysia, Selangor Darul Ehsan, Malaysia
[b] Centre of Foundation Studies for Agricultural Science, Universiti Putra Malaysia, Selangor Darul Ehsan, Malaysia
[c] Department of Mathematics, Faculty of Science, Universiti Putra Malaysia, Selangor Darul Ehsan, Malaysia

Original scientific paper
https://doi.org/10.2298/TSCI211104055M

The thermal properties of radiating water-based hybrid nanofluid with nanoparticles $Cu-Al_2O_3$ over an inclined shrinking plane are investigated. The governing equations in this model are transformed into similarity equations. Then, the boundary value problem solver (bvp4c) in MATLAB software is used numerically to solve these similarity equations. It has been discovered that utilizing MATLAB software the dual numerical solution occurs for certain values of the nanoparticle volume fraction and the suction parameter. Therefore, the skin friction coefficient and Nusselt number increase due to the effect of radiation and suction parameter. As a result of the findings, we were able to identify that the increasing nanoparticle volume fraction and the suction parameter cause the reliable numerical findings for velocity profile to enhance. When the first solution of suction parameter is increased, the skin friction coefficient and the local Nusselt number increase. Meanwhile, in the presence of the radiation parameter, the temperature of both solutions rises.

Key words: *hybrid nanofluid, thermal radiation, shrinking inclined plane, Al_2O_3, copper, suction*

Introduction

Thermal properties have significant contributions in different kinds of engineering and industrial applications. Wheelchair ramp and water heater using solar are examples of inclination sheets in an engineering application. The previous research paper considered the case of inclination case on the flat plane [1, 2]. However, research on the inclined plane is sparse. Hence, this article investigates the flow on an inclined plane at various angles using boundary-layer approximations. In addition, the heat and mass transfer bounded by inclined shrinking/stretching have been reported [3, 4].

Nanofluids were first introduced by Choi and Eastman [5], whereas the thermal conductivity variations on nanofluids were published [6-8]. The most recent research on nanofluids was conducted by [9-14], who included the following factors:

* Corresponding author, e-mail: ctsuzilliana@upm.edu.my

– the MHD case [9-11],
– different shape of container, such as trapezoidal cavity [9] and rectangular cavity [12],
– double-diffusive convection flow [10],
– with the existence of chemical reaction [13], and
– the occurrence of two heat sources [14].

Nowadays, researchers are more interested in hybrid nanofluids, which are considered revolutionary new in fluid dynamics. This type of nanofluids comprises two different nanoparticles dispersed in the base fluid [15]. Many scholars have explored further explorations of hybrid nanofluids in various flow configurations [16-21]. In their fluid-flow model, these publications [16-21] considered a magnetic field, buoyancy force, or stagnation point impact. Meanwhile, the effect of various nanoparticles in hybrid nanofluid has been described clearly in these publications [22-25], by considering these nanoparticles: Cu, Al_2O_3, TiO_2, molybdenum disulfide (MoS_2), Ag, and CuO (copper(II) oxide). Furthermore, thermal radiation can substantially impact temperature profiles and heat transfer rate at high pressure and temperature. Wakif *et al.* [26] explored the effects of thermal radiation on the thermomagneto-hydrodynamic stability of moving alumina nanoparticles in hybrid nanofluids containing copper oxide. Waqas *et al.*, [27] has also considered thermal radiation with magnetized flow over a vertical stretching cylinder in a hybrid nanofluid. They discovered that higher values of the porosity variable increase the temperature profile and suppress the fluid-flow.

According to the existing literature, there has been no previous investigation in hybrid nanofluid-flow on an inclined shrinking plane in the presence of thermal radiation and suction. A mathematical description of current research is built by referencing prior research from Waini *et al.* [15] to bridge the gap with the existing literature. Thus, utilizing an inclined plane, this paper will extend the analysis of the flat plane model by Waini *et al.* [15]. This paper investigates the effect of nanoparticle volume fraction parameter and temperature-dependent viscosity on the Nusselt number, skin friction coefficient, velocity profile, and temperature profile.

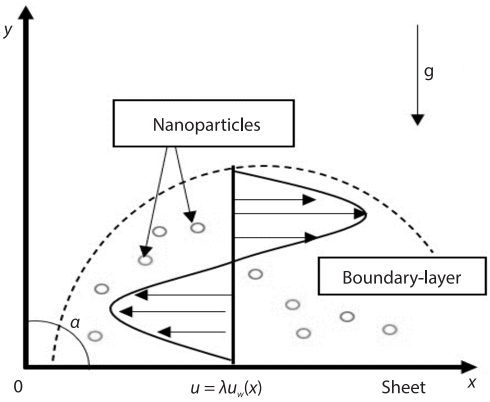

Figure 1. Schematic diagram

Mathematical formulation

The x-y cartesian co-ordinate of the fluid-flow model is depicted in fig. 1. The shrinking plane is projected by ∝ from the reference plate located at x-plane, and the y-axis parallel to the plane when $y = 0$. This model is under the influence of gravitational acceleration, g. In addition, the plane velocity is denoted by u_w, and the shrinking rate is indicated by λ. The velocity component of the hybrid nanofluids in directions along x and y are indicated with u and v. In this early formulation, a nanoparticle is neglected [15] since the mixture of the nanoparticles and the base fluid is stable. In this study, it was discovered that the shrinking case has occurred when $\lambda < 0$, whereas the plane remained static when $\lambda = 0$.

The following formulations are used for the governing boundary-layer equations of motion and the energy equation [28-31]:

$$\frac{\partial u}{\partial x}+\frac{\partial v}{\partial y}=0 \tag{1}$$

$$\frac{\partial u}{\partial x}+v\frac{\partial u}{\partial y}=\frac{\mu_{\mathrm{hnf}}}{\rho_{\mathrm{hnf}}}\frac{\partial^2 u}{\partial y^2}+\mathrm{g}\beta_T\left(T-T_\infty\right)\cos\alpha \tag{2}$$

$$u\frac{\partial T}{\partial x}+v\frac{\partial T}{\partial y}=\frac{\kappa_{\mathrm{hnf}}}{\left(\rho C_p\right)_{\mathrm{hnf}}}\frac{\partial^2 T}{\partial y^2}-\frac{1}{\left(\rho C_p\right)_{\mathrm{hnf}}}\frac{\partial q_r}{\partial y} \tag{3}$$

The boundary conditions are:

$$\begin{gathered} v=v_w\left(x\right),\ u=u_w\left(x\right)\lambda,\ T=T_w \ \text{ at } \ y=0 \\ y\to 0,\ T\to T_\infty,\ y\to\infty \end{gathered} \tag{4}$$

where $v_w(x)$ is the mass flux velocity, μ_{hnf} – the dynamic viscosity of the hybrid nanofluids, ρ_{hnf} – the density of the hybrid nanofluid, β_T – the coefficient of the thermal expansion, T – the fluid temperature, T_w – the surface temperature, T_∞ – the temperature far from the sheet, κ_{hnf} – the thermal conductivity of the hybrid nanofluid, and $(\rho C_p)_{\mathrm{hnf}}$ – the heat capacity of the hybrid nanofluids. For this study, the radiation flux, q_r – depicted from [32, 33]:

$$q_r=-\frac{4\sigma^*}{3k^*}\frac{\partial T^4}{\partial y} \tag{5}$$

where σ^* is called the Stefan-Boltzmann constant and k^* – the Rosseland absorption coefficient of the approximation. Besides, T^4 is the term where it can be joint as a linear function of temperature and can be expanded with Taylor series method. Next, the higher order is removed [32, 33], and the result:

$$T^4=4T_\infty^3T-3T_\infty^4 \tag{6}$$

Hence, the energy eq. (3) is expressed:

$$u\frac{\partial T}{\partial x}+v\frac{\partial T}{\partial y}=\left[\frac{\kappa_{\mathrm{hnf}}}{\left(\rho C_p\right)_{\mathrm{hnf}}}+\frac{16\sigma^*T_\infty^3}{3\left(\rho C_p\right)_{\mathrm{hnf}}k^*}\right]\frac{\partial^2 T}{\partial y^2} \tag{7}$$

where the fluid velocity is low due to the laminar flow, and viscous heat dissipation is expected to be minimal. Das [34] gives the effective basic nanofluids properties:

$$\begin{gathered} \rho_{\mathrm{nf}}=\left(1-\phi\right)\rho_{\mathrm{f}}+\phi\rho_{\mathrm{s}},\ \mu_{\mathrm{nf}}=\frac{\mu_{\mathrm{f}}}{\left(1-\phi\right)^{2.5}} \\ \left(\rho C_p\right)_{\mathrm{nf}}=\left(1-\phi\right)\left(\rho C_p\right)_{\mathrm{f}}+\phi\left(\rho C_p\right)_{\mathrm{s}},\ \frac{\kappa_{\mathrm{nf}}}{\kappa_{\mathrm{f}}}=\frac{\left(2\kappa_{\mathrm{f}}+\kappa_s\right)-2\phi\left(\kappa_{\mathrm{f}}-\kappa_s\right)}{\left(2\kappa_{\mathrm{f}}+\kappa_s\right)+\phi\left(\kappa_{\mathrm{f}}-\kappa_s\right)} \end{gathered} \tag{8}$$

where ρ is the density, μ – the viscosity, κ – the effective thermal conductivities, ϕ – the solid volume fraction, and (ρC_p) – the specific heat capacity. From eq. (8), subscripts nf, f, and s refer to the nanofluid, base fluid, and the nanoparticle, respectively.

Subsequently, the particular form of thermophysical characteristics [15] is used. The thermal parameters of the hybrid nanofluid that will be used in this study are listed in tab. 1, where subscript hnf refer to the symbols owned by hybrid nanofluid. Table 2 also includes the thermophysical characteristics of nanoparticles and the base fluid. The physical properties related to water (base fluid), Al_2O_3, and Cu for hybrid nanoparticles are given in tab. 2 [35, 36].

Table 1. Thermophysical properties of hybrid nanofluid [15-37]

Properties	Hybrid nanofluid
Dynamic viscosity	$\mu_{\text{hnf}} = \dfrac{\mu_{\text{f}}}{(1-\phi_1)^{2.5}(1-\phi_2)^{2.5}}$
Thermal conductivity	$\dfrac{\kappa_{\text{hnf}}}{\kappa_{\text{f}}} = \dfrac{(2\kappa_{\text{nf}}+\kappa_{\text{s2}})-2\phi_2(\kappa_{\text{nf}}-\kappa_{\text{s2}})}{(2\kappa_{\text{nf}}+\kappa_{\text{s2}})+\phi_2(\kappa_{\text{nf}}-\kappa_{\text{s2}})}$ where $\dfrac{\kappa_{\text{hnf}}}{\kappa_{\text{f}}} = \dfrac{(2\kappa_{\text{f}}+\kappa_{\text{s1}})-2\phi_1(\kappa_{\text{f}}-\kappa_{\text{s1}})}{(2\kappa_{\text{f}}+\kappa_{\text{s1}})+\phi_1(\kappa_{\text{f}}-\kappa_{\text{s1}})}$
Density	$\rho_{\text{hnf}} = (1-\phi_2)\left[(1-\phi_1)\rho_f + \phi_1\rho_{\text{s1}}\right] + \phi_2\rho_{\text{s2}}$
Heat capacity	$(\rho C_p)_{\text{hnf}} = (1-\phi_2)\left[(1-\phi_1)(\rho C_p)_{\text{f}} + \phi_1(\rho C_p)_{\text{s1}}\right] + \phi_2(\rho C_p)_{s2}$

Table 2. Thermophysical properties [35, 36]

	ρ [kgm^{-3}]	C_p [Jkg^{-1}K^{-1}]	κ [Wm^{-1}K^{-1}]
Water	997.1	4179	0.613
Al_2O_3	3970	765	40
Cu	8933	385	400

The similarity variables are used to reduce the aforementioned governing equations depicted from [15]:

$$u = \frac{\nu_f}{L^{\frac{4}{3}}} x^{1/3} f'(\eta), \quad v = -\frac{1}{3}\frac{\nu_f}{L^{2/3}} x^{-1/3}\left[2f(\eta) - \eta f'(\eta)\right] \tag{9}$$

$$\theta(\eta) = \frac{T - T_\infty}{T_w - T_\infty}, \ \ \eta = y\frac{x^{-1/3}}{L^{2/3}} \tag{10}$$

where η is the similarity variable and L – the length of characteristic.

We assumed:

$$u_w(x) = \left(\frac{\nu_{\text{f}}}{L^{2/3}}\right)x^{1/3}, \ \ v_w = -\frac{1}{3}\frac{\nu_{\text{f}}}{L^{2/3}} x^{-1/3}\left[2f(\eta) - \eta f'(\eta)\right]S \tag{11}$$

where S is the steady mass flux parameter, with $S > 0$ indicating suction.

In our study, substituting eqs. (7)-(10) into eqs. (2) and (7) give:

$$\frac{\dfrac{\mu_{\text{hnf}}}{\mu_{\text{f}}}}{\dfrac{\rho_{\text{hnf}}}{\rho_{\text{f}}}} 3f''' + 2ff'' - f'^2 + \varepsilon\theta\cos\alpha = 0 \tag{12}$$

$$\frac{3}{\Pr}\frac{\dfrac{\kappa_{\text{hnf}}}{\kappa_{\text{f}}}}{\dfrac{\left(\rho C_p\right)_{\text{hnf}}}{\left(\rho C_p\right)_{\text{f}}}}\left[1+\frac{4}{3\dfrac{\kappa_{\text{hnf}}}{\kappa_{\text{f}}}}R\right]\theta''+2f\theta'=0 \tag{13}$$

The boundary conditions are transformed as given:

$$f\left(0\right)=S,\ f'\left(0\right)=\lambda,\ \theta\left(0\right)=1,\ f'\left(\infty\right)\to 0,\ \theta'\left(\infty\right)\to 0 \tag{14}$$

where

$$R=\frac{4\sigma^{*}T_{\infty}^{3}}{(\kappa)(\kappa_{f})}$$

for the radiation parameter, Pr = $\mu_{\text{f}}(C_p)f/\kappa_{\text{f}}$ for Prandtl number, and ε is the mixed convection parameter. The primes in eqs. (11) and (12) denote the function differentiation with respect to η. The skin friction coefficients, C_f and the Nusselt number, Nu_x, are the physical parameters of primary interest in practical applications, which are defined:

$$C_f=\frac{\tau_w}{\rho_{\text{f}}u_w^2},\ \text{Nu}_x=\frac{xq_w}{\kappa_{\text{f}}\left(T_w-T_\infty\right)} \tag{15}$$

and given:

$$\tau_w=\mu_{\text{hnf}}\left(\frac{\partial u}{\partial y}\right)_{y=0},\ q_{\text{w}}=-\kappa_{\text{hnf}}\left(\frac{\partial T}{\partial y}\right)_{y=0}+\left(q_r\right)_{y=0} \tag{16}$$

where τ_w is the shear stress along the plate and q_w – the heat flux from the plate. The skin friction and Nusselt number can be ordered by substituting eqs. (7)-(9) into eqs. (14) and (15) to get:

$$C_f\text{Re}_x^{1/2}=\frac{\mu_{\text{hnf}}}{\mu_{\text{f}}}f''\left(0\right),\ \text{Nu}_x\,\text{Re}_x^{1/2}=-\left(\frac{\kappa_{\text{hnf}}}{\kappa_{\text{f}}}+\frac{4}{3}R\right)\theta'\left(0\right) \tag{17}$$

where

$$\text{Re}_x=\frac{u_w\left(x\right)x}{\nu_{\text{f}}}$$

is called the local Reynold numbers.

Result and discussion

Equations (12) and (13) has been analysed with inclined permeable shrinking sheet using bvp4c MATLAB software with the boundary conditions in eq. (14). This study adds Al_2O_3 (first nanoparticles) with Cu (second nanoparticles) to form a water-based hybrid nanofluid. The first and second nanoparticles are denoted by ϕ_1 and ϕ_2, respectively. The present study shows several fixed parameters which have been identified: Prandtl number Pr = 6.2, first nanoparticle volume fraction ϕ_1 = 0.01, second nanoparticle volume fraction ϕ_2 = 0.06, thermal radiation R = 1.0 suction, S = 2.2, shrinking sheet λ = –1.0, inclined angle alpha α = 45°, and mixed convection parameter ϵ = 0.05. The results presented here are subjected to the various values of Cu nanoparticles, instead of Al_2O_3 [15]. The various values of parameters such ϕ_2, S, and R have been observed for the velocity and temperature profiles in figs. 2-6, respectively. Moreover, the C_f and Nusselt number also will be displayed in figs. 7 and 8, with the impacts of ϕ_2 and S. Dual solutions are introduced in the graph denoted as first solution (solid line) and second solution (dashed line).

Figures 2 and 3 presents the dual solutions of velocity profiles $f'(\eta)$ and temperature profiles $\theta(\eta)$, with distinct values ϕ_2. The obtained results in figs. 2 and 3 show that increases ϕ_2 leads to a rise in fluid velocity and temperature profiles for the first solution, while the velocity profile decreases for the second solution. This result is due to the presence of the inclined permeable shrinking sheet, which makes the first solution slightly thicker than the second solution in different ϕ_2.

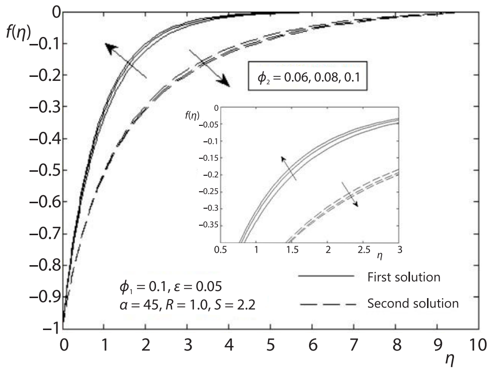

Figure 2. Various values of ϕ_2 for $f'(\eta)$

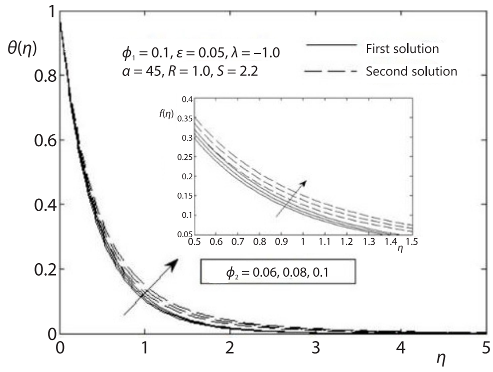

Figure 3. Various values of ϕ_2 for $\theta(\eta)$

Next, fig. 4 shows the $f'(\eta)$ and $\theta(\eta)$ for the difference in S = 2.15, 2.20, 2.25. From the graph observation, fig. 4 displays that increasing S can cause an increase in velocity profiles. For the initial solutions, the temperature profile in fig. 5 is rising. On the other hand, fig. 4 differs in the second solution where the decrease in velocity profile and temperature profile identified due to an increase in suction parameter, S. This finding is because suction creates greater resistance in fluid-flow as stated by [37].

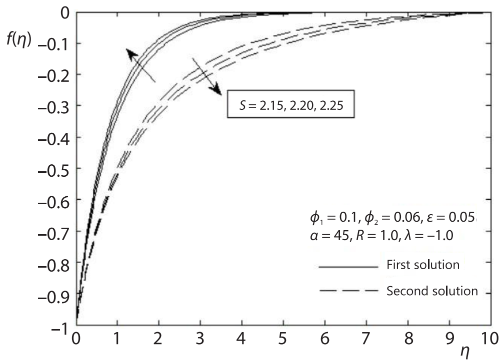

Figure 4. Various values of S for $f'(\eta)$

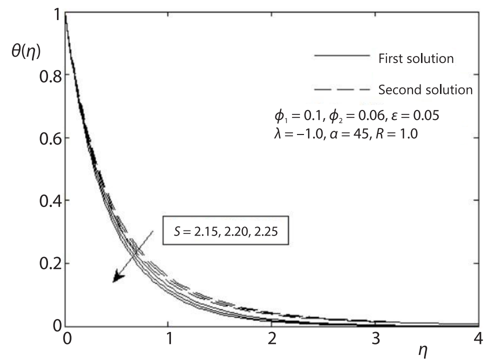

Figure 5. Various values of S for $\theta(\eta)$

Furthermore, the graph of temperature profile with different values of thermal radiation, R, are shown in fig. 6. As a result, with an increase in R, the value of temperature profile, $\theta(\eta)$ will also increase for dual solutions. It can be identified that the thermal boundary-layer thickness is enhanced due to the increase in R. Therefore, the higher the values of R indicates that more radiative heat energy is pumped into the flow field causes the increment in temperature.

Next, figs. 7 and 8 describe the C_f, $f''(0)$, and Nusselt number with various values of nanoparticle volume fraction for ϕ_2. Figure 7 demonstrate the various values of S on $f''(0)$ when dealing with different values of ϕ_2. From fig. 7, the intersection point is introduced as a critical suction point S_c and can be seen smoothly intersecting for the first solution and second solution. From the observation, the increase in suction parameter, S, and nanoparticle volume fraction for ϕ_2 leads to the increase in C_f for first solution. This result is because mass suctions can aid the passage of hybrid fluid particles toward the wall while also causing the flow to move more slowly as proved by [17]. Besides, the second solution is *vice versa* from the first solution from observation. We can see that as ϕ_2 increases, the solution domain grows and the crucial values S_c shift to the left. Furthermore, for the upper branch solutions, the values of $f''(0)$ grow as S_c increases. As a result, the value of critical suction for dual solutions from fig. 7 are 2.1142 ($\phi_2 = 0.06$), 2.0871 ($\phi_2 = 0.08$), and 2.0686 ($\phi_2 = 0.1$).

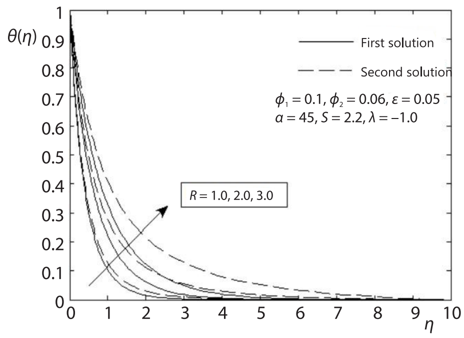

Figure 6. Various values of R for $\theta(\eta)$

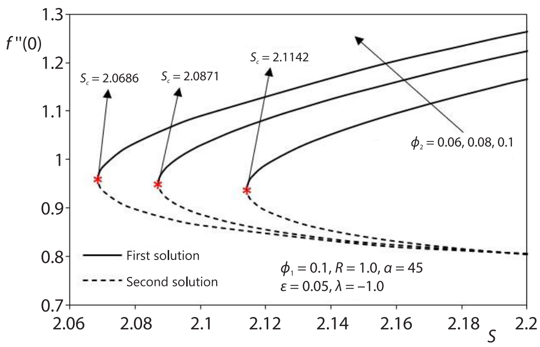

Figure 7. Various values of ϕ_2 for $f''(0)$ with S

From fig. 8, the Nusselt number has been presented when $\phi_2 = 0.06$ and $S_c = 2.1142$. The illustration of Nusselt number for other ϕ_2 ($\phi_2 = 0.08$ and 0.1) are not attached here due to the pages limitation. However, their variation have remained the same (the first solution decreases when it is approaching the critical point S_c, whereas the second solution enhances). The critical suction points for fig. 8 have remained the same as fig. 7: $S_c = 2.1142$, $S_c = 2.0871$, $S_c = 2.0686$ when $\phi_2 = 0.06$, 0.08, 0.1, respectively. From this information, the increase in ϕ_2 and S leads to the increase in the Nusselt number for the first solution, while the Nusselt number in the second solution is decreased.

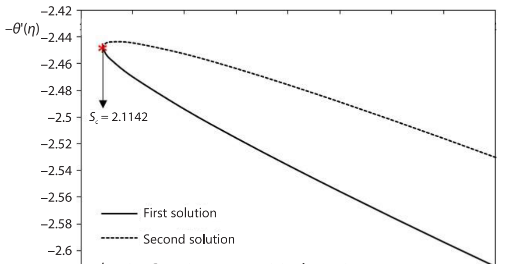

Figure 8. The variation of $-\theta'(\eta)$ with S when $\phi_2 = 0.06$

Conclusion

The governing boundary-layer equations have been reduced to ODE with the appropriate similarity transformation before being solved using bvp4c and programmed in MATLAB software. In this study, the first and second solutions indicate the different solutions in the graph for various parameters. As a result, we can conclude that the velocity profile increases for the first solutions when the nanoparticle volume fraction ϕ_2 and suction parameter S also increase.

It was observed that as the suction parameter was increased, the temperature of both solutions decreased. While the increase in temperature profile leads to the rise in thermal radiation, R. The effects of the thermal radiation parameter, R, thicken the thermal boundary-layer for both solutions, as well. Moreover, the C_f and Nusselt number increase, which make the suction parameter and nanoparticle volume fraction ϕ_2 increases.

Acknowledgment

This research was funded by a grant from the Ministry of Higher Education of Malaysia through Fundamental Research Grant Scheme FRGS/1/2020/STG06/UPM/02/1.

Nomenclature

C_f – skin friction coefficient
C_p – specific heat at constant pressure, [$\mathrm{Jkg^{-1}K^{-1}}$]
$f(\eta)$ – dimensionless stream function
g – gravitational acceleration, [$\mathrm{ms^{-2}}$]
k^* – Rosseland mean absorption coefficient, [$\mathrm{m^{-1}}$]
L – characteristics length of the surface, [m]
Nu_x – local Nusselt number
Pr – Prandtl number
q_r – radiative heat flux component in y-directions, [$\mathrm{Wm^{-2}}$]
q_w – surface heat flux, [$\mathrm{Wm^{-2}}$]
R – radiation parameter
Re_x – local Reynolds number
S – suction parameter
T – fluid temperature, [K]
T_w – surface temperature, [K]
T_∞ – ambient temperatute, [K]
u, v – velocity of components in the x- and y-directions, [$\mathrm{ms^{-1}}$]
u_w – velocity of shrinking surface, [$\mathrm{ms^{-1}}$]
u_∞ – velocity of the mainstream, [$\mathrm{ms^{-1}}$]
v_w – mass flux velocity, [$\mathrm{ms^{-1}}$]
x, y – cartesian co-ordinates, [m]

Greek symbol

α – inclined angle of the shrinking sheet, [°]
β_T – coefficient of the thermal expansion, [$\mathrm{K^{-1}}$]
η – similarity variable
θ – dimensionless temperature
κ – effective thermal conductivity, [$\mathrm{Wm^{-1}K^{-1}}$]
κ_{hnf} – thermal conductivity of the hybrid nanofluid, [$\mathrm{Wm^{-1}K^{-1}}$]
ε – mixed convection parameter.
λ – constant shrinking parameter
μ_{hnf} – dynamic viscosity (hybrid nanofluid), [$\mathrm{kgm^{-1}s^{-1}}$]
ρ_{hnf} – density (hybrid nanofluid), [$\mathrm{kgm^{-3}}$]
$\rho(C_p)_{\mathrm{hnf}}$ – heat capacitance of the hybrid nanofluid, [$\mathrm{JK^{-1}m^{-3}}$]
ν_{f} – kinematic viscosity of the base fluid, [$\mathrm{m^2s^{-1}}$]
σ^* – constant of Stefan-Botlzmann, [$\mathrm{Wm^{-2}K^{-4}}$]
ϕ_1 – nanoparticle volume fractions (Al_2O_3)
ϕ_2 – nanoparticle volume fractions (Cu)
τ_w – skin friction, [$\mathrm{kgm^{-1}s^{-2}}$]

Subscripts

f – fluid
nf – nanofluid
hnf – hybrid nanofluid
s – nanoparticles

Superscript

′ – differentiation with respect to η

References

[1] Rout, B. R., *et al.*, The MHD Heat and Mass Transfer of Chemical Reaction Fluid-Flow over a Moving Vertical Plate in Presence of Heat Source with Convective Surface Boundary Condition, *International Journal of Chemical Engineering*, *2013* (2013), ID296834
[2] Hamad, M. A. A., *et al*., Magnetic Field Effects on Free Convection Flow of a Nanofluid Past a Vertical Semi-Infinite Flat Plate, Non-Linear Analysis, *Real World Applications*, *12* (2011), 3, pp. 1338-1346
[3] Azmi, H. M., *et al*., The Boundary-Layer Flow, Heat and Mass Transfer beyond an Exponentially Stretching/Shrinking Inclined Sheet, *CFD Letters*, *12* (2020), 8, pp. 98-107
[4] Parvin, S., *et al.*, The Inclined Factors of Magnetic Field and Shrinking Sheet in Casson Fluid-Flow, *Heat and Mass Transfer Symmetry*, *13* (2021), 3, 373
[5] Choi, S. U., Eastman, J. A., Enhancing Thermal Conductivity of Fluids with Nanoparticles, *Proceedings*, ASME International Mechanical Engineering Congress and Exhibition, San Francisco, Cal., USA, 1995, Vol. 66, pp. 99–105

[6] Pil Jang, S., Choi, S. U., Effects of Various Parameters on Nanofluid Thermal Conductivity, *Journal of Heat Transfer*, *129* (2007), 5, pp. 617-623
[7] Ismail, H. N., *et al*., Effect of Variable Thermal Conductivity on the MHD Boundary-Layer of Casson-Nanofluid over a Moving Plate with Variable Thickness, *Thermal Science*, *25* (2021), 1A, pp. 145-157
[8] Ullah Khan, S., *et al.*, Thermo Diffusion Aspects in Jeffrey Nanofluid over Periodically Moving Surface with Time Dependent Thermal Conductivity, *Thermal Science*, *25* (2021), 1A, pp. 197-207
[9] Mondal, P., Mahapatra, T. R., The MHD Double-Diffusive Mixed Convection and Entropy Generation of Nanofluid in a Trapezoidal Cavity, *International Journal of Mechanical Sciences*, *208* (2021), 106665
[10] Parvin, S., *et al*., Numerical Treatment of 2-D-Magneto Double-Diffusive Convection Flow of a Maxwell Nanofluid: Heat Transport Case Study, *Case Studies in Thermal Engineering*, *28* (2021), 101383.
[11] Mahdy, A. E. N., *et al*., Unsteady Homogeneous-Heterogeneous Reactions in MHD Nanofluid Mixed Convection Flow Past a Stagnation Point of an Impulsively Rotating Sphere, *Thermal Science*, *25* (2021), 1A, pp. 243-256
[12] Lafdail, Z., et al., Numerical Study of Turbulent Natural-Convection of Nanofluids in Differentially Heated Rectangular Cavities, *Thermal Science*, *25* (2021), pp. 579-589
[13] Eldabe, N. T., et al., Analytical and Numerical Treatment to Study the Effects of Hall Currents with Viscous Dissipation, Heat Absorpation and Chemical Reaction on Peristaltic Flow of Carreau Nanofluid *Thermal Science*, *25* (2021), 1B, pp. 181-196
[14] Ghaneifar, M., *et al*., Mixed Convection Heat Transfer of Al_2O_3 Nanofluid in a Horizontal Channel Subjected with Two Heat Sources, *Journal of Thermal Analysis and Calorimetry*, *143* (2021), 3, pp. 2761-2774
[15] Waini, I., *et al*., Hybrid Nanofluid-Flow and Heat Transfer over a Non-Linear Permeable Stretching/Shrinking Surface, *International Journal of Numerical Methods for Heat & Fluid-Flow*, *29* (2019), 9, pp. 3110-3127
[16] Zainal, N. A., *et al.*, The MHD Mixed Convection Stagnation Point Flow of a Hybrid Nanofluid Past a Vertical Flat Plate with Convective Boundary Condition, *Chinese Journal of Physics*, *66* (2020), Aug., pp. 630-644
[17] Anuar, N. S., *et al*., Influence of buoyancy Force on Ag-MgO/Water Hybrid Nanofluid-Flow in an Inclined Permeable Stretching/Shrinking Sheet, *International Communications in Heat and Mass Transfer*, *123* (2021), 105236
[18] Yashkun, U., *et al*., The MHD Hybrid Nanofluid-Flow over a Permeable Stretching/Shrinking Sheet with Thermal Radiation Effect, *International Journal of Numerical Methods for Heat & Fluid-Flow*, *31* (2021), 3, pp. 1014-1031
[19] Nadeem, S., *et al.*, Inspection of Hybrid Based Nanofluid-Flow over a Curved Surface, *Computer Methods and Programs in Biomedicine*, *189* (2020), 105193
[20] Lund, L. A., *et al*., Stability Analysis and Multiple Solution of Cu-Al_2O_3/H_2O Nanofluid Contains Hybrid Nanomaterials over a Shrinking Surface in the Presence of Viscous Dissipation, *Journal of Materials Research and Technology, 9* (2020), 1, pp. 421-432
[21] Ashorynejad, H. R., Shahriari, A., The MHD Natural-Convection of Hybrid Nanofluid in an Open Wavy Cavity, *Results in Physics*, *9* (2018), June, pp. 440-455
[22] Arani, A. A. A., Aberoumand, H., Stagnation-Point Flow of Ag-CuO/Water Hybrid Nanofluids over a Permeable Stretching/Shrinking Sheet with Temporal Stability Analysis, *Powder Technology*, *380* (2021), 21, pp. 152-163
[23] Waini, I., *et al*., Stagnation Point Flow Toward an Exponentially Shrinking Sheet in a Hybrid Nanofluid, *International Journal of Numerical Methods for Heat & Fluid-flow*, *32* (2022), 3, pp. 1012-1014
[24] Jamshed, W., *et al*., Thermal Growth in Solar Water Pump Using Prandtl-Eyring Hybrid Nanofluid: A Solar Energy Application, *Scientifc Reports*, *11* (2021), 18704
[25] Jamshed, W., *et al*., Computational Case Study on Tangent Hyperbolic Hybrid Nanofluid-Flow: Single Phase Thermal Investigation, *Case Studies in Thermal Engineering*, *27* (2021), 101246
[26] Wakif, A., *et al.*, Thermal Radiation and Surface Roughness Effects on the Thermo-Magneto-Hydrodynamic Stability of Alumina-Copper Oxide Hybrid Nanofluids Utilizing the Generalized Buongiorno's Nanofluid Model, *Journal of Thermal Analysis & Calorimetry*, *143* (2021), Mar., pp. 1201-1220
[27] Waqas, H., *et al.*, Thermal Transport in Magnetized Flow of Hybrid Nanofluids over a Vertical Stretching Cylinder, *Case Studies in Thermal Engineering*, *27* (2021), 101219
[28] Tiwari., *et al.*, Heat Transfer Augmentation in a Two-Sided Lid-Driven Differentially Heated Square Cavity Utilizing Nanofluids, *International Journal of Heat and Mass Transfer*, 50 (2007), 9-10, pp. 2002- 2018

[29] Cortell, R., Heat and Fluid-Flow Due to Non-Linearly Stretching Surfaces, *Applied Mathematics and Computation 21* (2011), 19, pp. 7564-7572
[30] Kazemi, M. A., *et al.*, Analytical Solution of Convective Heat Transfer of a Quiescent Fluid over a Non-Linearly Stretching Surface Using Homotopy Analysis Method, *Results in Physics*, *10* (2018), Sept., pp. 164-172
[31] Waini, I., *et al*., Hybrid Nanofluid-Flow Induced by an Exponentially Shrinking sheet, *Chinese Journal of Physics*, *68* (2020), Dec., pp. 468-482
[32] Roselland, S., *Astrophysik Und Atom-Theoretische Grundlagen* (in German), Springer-Verlag, Berlin, Germany, 1931 pp. 41-44
[33] Pal, D., Mondal., H., Influence of Temperature-Dependent Viscosity and Thermal Radiation on MHD Forced Convection over a Non-Isothermal Wedge, *Applied Mathematics and Computation*, *212* (2009), 1, pp. 194-208
[34] Das, K., Cu-Water Nanofluid-Flow and Heat Transfer over a Shrinking Sheet, *Journal of Mechanical Science and Technology*, *28* (2014), 12, pp. 5089-5094
[35] Oztop, H. F., Abu-Nada, E., Numerical Study of Natural-Convection in Partially Heated Rectangular Enclosures Filled with Nanofluids, *International Journal of Heat and Fluid-Flow, 29* (2008), 5, pp. 1326-1336
[36] Hussain, S., *et al.*, Entropy Generation Analysis in MHD Mixed Convection of Hybrid Nanofluid in an Open Cavity with a Horizontal Channel Containing an Adiabatic Obstacle, *International Journal of Heat and Mass Transfer, 114* (2017), Nov., pp. 1054-1066
[37] Lund, L. A., *et al.*, Stability Analysis and Multiple Solution of Cu-Al_2O_3/H_2O Nanofluid Contains Hybrid Nanomaterials over a Shrinking Surface in the Presence of Viscous Dissipation, *Journal of Materials Research and Technology*, *9* (2020), 1, pp. 421-432

Paper submitted: November 4, 2021
Paper revised: February 15, 2022
Paper accepted: March 2, 2022